Supplementary material for

Selective and sensitive detection of CO_2 using phosphorescent iridium(III) complexes containing 1,10-phenanthroline derivatives as neutral ligands

Xiaoxue Liu, Xi Chu, Chenghao Li, Hongyi Liu, Yihao Zheng, Hongyan Li*

School of Chemical Engineering and Technology, Hebei University of Technology, Tianjin, 300401, China

* Corresponding authors.

E-mail address: hyli@hebut.edu.cn

Figures and Tables captions

Experimental Section

Fig. S1. The ^{1}H NMR spectrum of the complex **1**.

Fig. S2. The ^{13}C NMR spectrum of the complex **1**.

Fig. S3. The ^{1}H NMR spectrum of the complex **2**.

Fig. S4. The ^{13}C NMR spectrum of the complex **2**.

Fig. S5. The ^{1}H NMR spectrum of the complex **3**.

Fig. S6. The ^{13}C NMR spectrum of the complex **3**.

Fig. S7. The ^{1}H NMR spectrum of the complex **4**.

Fig. S8. The ^{13}C NMR spectrum of the complex **4**.

Fig. S9. The ^{1}H NMR spectrum of the complex **5**.

Fig. S10. The ^{13}C NMR spectrum of the complex **5**.

Fig. S11. The ^{1}H NMR spectrum of the complex **6**.

Fig. S12. The ^{13}C NMR spectrum of the complex **6**.

Fig. S13. The ^{1}H NMR spectrum of the complex **7**.

Fig. S14. The ^{13}C NMR spectrum of the complex **7**.

Fig. S15. The ^{1}H NMR spectrum of the complex **8**.

Fig. S16. The ^{13}C NMR spectrum of the complex **8**.

Fig. S17. Photoluminescence spectra of **1** upon addition of various anions (3.0 equiv.) in acetonitrile solution.

Fig. S18. Photoluminescence spectra of **5** upon addition of various anions (3.0 equiv.) in acetonitrile solution.

Fig. S19. The phosphorescence responses of complexes **5** in the presence of CH_3COO^- and then bubbling excess O_2, N_2, Ar, and CO gas.

Fig. S20. The anti-interference experiment results of complex **5** in the presence of CH_3COO^- for sensing CO_2.

Fig. S21. Phosphorescence intensity change of **1−CH_3COO^-** (left) and complex

5−CH_3COO^- symstem (5 μM) upon bubbling with various quantities of CO_2.

Table S1 The frontier orbital energy and electron density distribution for complexes **1–8**.

Table S2 Main experimental and calculated optical transitions for complexes **1–8.**

Table S3 The coordination geometry used to detect CO_2 and its corresponding detection limits

1. Experimental

1.1 General procedures

All reagents and chemicals were obtained from commercial sources and used as received without further purification. In order to avoid the interference from the difference of cations, the corresponding tetrabutylammonium salts of CH_3COO^-, F^-, Br^-, I^-, SO_4^{2-}, HSO_4^-, NO_3^-, Cl^- were chosen to prepare the anionic solution used in the experiments. The ^1H and ^{13}C NMR spectra were acquired at 298 K on the Bruker AM 400 MHz instrument. Elemental analyses were performed by FLASHEA 112 Series. Electrospray ionization mass spectrometric (ESI-MS) measurements were made on Agilent 6520 Q-TOF LC/MS. Absorption and photoluminescence spectra were recorded by a UV-2700 spectrophotometer and Hitachi F-2700 photoluminescence spectrophotometer. Edinburgh Instruments FLS920P fluorescence spectrometer was used to measure the phosphorescence lifetimes of the complexes. The photoluminescent quantum yield were calculated according to the equation by comparing the emission intensity (integral areas) of the standard sample ($Ir(ppy)_3$) with that of the unknown sample. The equation is as follows.

$$\boldsymbol{\Phi_{unk} = \Phi_{std}(\frac{I_{unk}}{I_{std}})(\frac{A_{std}}{A_{unk}})\left(\frac{\eta_{unk}}{\eta_{std}}\right)^2}$$

Where the subscripts for unk and std represent the unknown sample and $Ir(ppy)_3$, respectively. The physical quantity I represents the integrated emission intensity of their solution, The physical quantity A represents the absorbance of their solution at their excitation wavelength, and the letter η represents the refractive indices of the corresponding solvents (pure solvents were assumed). The Φ_{std} of $Ir(ppy)_3$ measured in oxygen-free dichloromethane solution at 298 K has been revalued to be 0.97 (error: ±10%).

1.2 Computational details

The Gaussian 09 software package was used to do all of the calculations. The density functional theory (DFT) and time-dependent DFT (TD-DFT) were carried out with no symmetry constraints to investigate optimized geometries and electron configurations with the Becke three-parameter Lee-Yang-Parr (B3LYP) hybrid density functional theory. Ir atoms were based on the LANL2DZ basis throughout all calculations, while all non-metallic atoms were based on the 6-31G (d, p) basis. Considering the influence of solvent effect, the polarized continuum model approach was used to simulate the interaction with solvent in the calculation process.

1.3 Synthesis of complexes 1–8

A mixture of the Ir(III) chloro-bridged dimers (1.0 equiv.) and the neutral ligand (1.1 equiv.) were refluxed 12 h at 70 ˚C in a mixed solvent (30 mL) of CH_2Cl_2 and CH_3OH (1:1, v:v) under nitrogen atmosphere. After cooling to room temperature, KPF_6 was added to the reaction solution and the mixture was continued to stir for 2 h. The solvent was evaporated under reduced pressure to obtain the crude product. The combined organic phase was concentrated and purified by column

chromatography using dichloromethane and methanol as the eluent (v / v = 20:1) to provide complexes **1**–**8**.

[$(F_4ppy)_2Ir(pip)$](PF_6) (**1**): 0.31 g (0.27 mmol) of $(F_4ppy)_2Ir(\mu\text{-}Cl)]_2$ and 0.18 g (0.62 mmol) of pip, and 0.53 g (2.88 mmol) of KPF_6 gave 0.41 g yellow powder. Yield: 77%. ^{1}H NMR (400 MHz, DMSO-d_6) δ 14.37 (s, 1H), 9.22 (s, 2H), 8.30 (s, 4H), 8.21 (s, 2H), 8.14–8.05 (m, 4H), 7.97–7.87 (m, 2H), 7.66(s, 2H), 7.61 (s, 1H), 7.50 (s, 2H), 7.02 (s, 2H), 6.93 (s, 2H), 5.88 (d, J = 7.2 Hz, 2H). ^{13}C NMR (101 MHz, DMSO-d_6) δ 166.18, 163.50 (d, J = 253.5 Hz), 153.92, 153.86, 153.28, 149.72, 149.24, 144.54, 141.10, 139.62, 133.02, 131.01, 129.82, 129.78, 127.98 (d, J = 10.1 Hz), 127.72, 127.10, 124.41, 120.71, 117.46 (d, J = 17.2 Hz), 110.20 (d, J = 23.2 Hz). MS (ESI) m/z: calcd for $[C_{42}H_{26}F_2IrN_6]^+$, 833.1816; found, 833.1811 $[M\text{-}PF_6]^+$.

[$(F_4piq)_2Ir(pip)$](PF_6) (**2**): 0.31 g (0.27 mmol) of $[(F_4piq)_2Ir(\mu\text{-}Cl)]_2$ and 0.18 g (0.62 mmol) of pip, and 0.53 g (2.88 mmol) of KPF_6 gave 0.41 g orange powder. Yield: 75%. ^{1}H NMR (400 MHz, DMSO-d_6) δ 14.38 (s, 1H), 9.21 (d, J = 7.8 Hz, 2H), 9.00 (d, J = 6.6 Hz, 2H), 8.57–8.50 (m, 2H), 8.31 (d, J = 7.4 Hz, 2H), 8.15–8.04 (m, 6H), 7.90 (d, J = 7.6 Hz, 4H), 7.67 (t, J = 7.0 Hz, 2H), 7.61 (d, J = 7.1 Hz, 1H), 7.47 (d, J = 6.3 Hz, 2H), 7.39 (t, J = 5.9 Hz, 2H), 7.04 (t, J = 8.2 Hz, 2H), 5.90 (d, J = 7.8 Hz, 2H). ^{13}C NMR (101 MHz, DMSO-d_6) δ 167.11, 163.28 (d, J = 256.5 Hz), 157.47, 153.40, 149.17, 144.35, 142.31, 141.15, 137.08, 133.50 (d, J = 9.1 Hz), 133.08, 132.75, 130.96, 130.86, 130.09, 129.97, 129.77, 128.26, 127.81, 127.12, 126.79, 125.88, 122.83, 117.90 (d, J = 16.2 Hz), 110.12 (d, J = 22.2 Hz). MS (ESI) m/z: calcd for $[C_{49}H_{30}F_2IrN_6]^+$, 933.2129; found, 933.2175 $[M\text{-}PF_6]^+$.

[$(F_4ppy)_2Ir(tfpip)$](PF_6) (**3**): 0.31 g (0.27 mmol) of $[(F_4ppy)_2Ir(\mu\text{-}Cl)]_2$ and 0.18 g (0.62 mmol) of tfpip, and 0.53 g (2.88 mmol) of KPF_6 gave 0.41 g yellow powder. Yield: 71%. ^{1}H NMR (400 MHz, DMSO-d_6) δ 14.65 (s, 1H), 9.23 (d, J = 7.0 Hz, 2H), 8.54 (d, J = 7.1 Hz, 2H), 8.28 (d, J = 7.1 Hz, 2H), 8.24 – 8.20 (m, 2H)., 8.08 (d, J = 8.3 Hz, 6H), 7.95–7.90 (m, 2H), 7.52–7.47 (m, 2H), 7.02 (s, 2H), 6.93 (s, 2H), 5.87 (d, J = 7.3 Hz, 2H):^{13}C NMR (101 MHz, DMSO-d_6) δ 166.18, 163.50 (d, J = 253.5 Hz), 153.82, 151.58, 149.73, 149.50, 144.81, 141.09, 139.64, 133.59, 133.11, 130.81, 130.49, 128.00 (d, J = 9.1 Hz), 127.71, 126.83, 124.41, 123.22, 120.73, 117.46 (d, J = 17.2 Hz), 110.21 (d, J = 22.2 Hz). MS (ESI) m/z: calcd for $[C_{42}H_{25}F_5IrN_6]^+$, 901.1690; found, 901.1701 $[M\text{−}PF_6]^+$.

[$(F_4piq)_2Ir(tfpip)$](PF_6) (**4**): 0.31 g (0.27 mmol) of $[(F_4piq)_2Ir(\mu\text{-}Cl)]_2$ and 0.18 g (0.62 mmol) of tfpip, and 0.53 g (2.88 mmol) of KPF_6 gave 0.41 g orange powder. Yield: 76%. ^{1}H NMR (400 MHz, DMSO-d_6) δ 14.61 (s, 1H), 9.19 (d, J = 7.1 Hz, 2H), 9.05–8.98 (m, 2H), 8.52 (s, 4H), 8.15 (s, 2H), 8.07 (d, J = 15.0 Hz, 6H), 7.92–7.86 (m, 4H), 7.47 (s, 2H), 7.41 (s, 2H), 7.04 (s, 2H), 5.93 (d, J = 7.7 Hz, 2H). ^{13}C NMR (101 MHz, DMSO-d_6) δ 167.10, 163.28 (d, J = 253.5 Hz), 157.43, 157.39, 151.62, 149.47, 144.64, 142.32, 141.18, 137.09, 133.64, 133.52 (d, J = 7.2 Hz), 133.18, 132.78, 130.79, 130.46, 130.11, 128.27, 127.71, 126.80, 125.87, 123.24, 122.84, 117.90 (d, J = 17.2 Hz), 110.16 (d, J = 23.2 Hz). MS (ESI) m/z: calcd for $[C_{50}H_{29}F_5IrN_6]^+$, 1001.2003; found, 1001.2070 $[M\text{-}PF_6]^+$.

$[(F_{3,5}ppy)_2Ir(pip)](PF_6)$ (**5**): 0.31 g (0.27 mmol) of $[(F_{3,5}ppy)_2Ir(\mu\text{-}Cl)]_2$ and 0.18 g (0.62 mmol) of pip, and 0.53 g (2.88 mmol) of KPF_6 gave 0.41 g yellow powder. Yield: 76%. ^{1}H NMR (400 MHz, DMSO-d_6) δ 9.22 (d, J = 8.2 Hz, 2H), 8.35–8.28 (m, 4H), 8.26 (d, J = 4.2 Hz, 2H), 8.13–8.05 (m, 2H), 7.92 (d, J = 8.9 Hz, 2H), 7.85 (t, J = 7.5 Hz, 2H), 7.65 (t, J = 6.9 Hz, 2H), 7.58 (d, J = 6.9 Hz, 1H), 7.43 (d, J = 5.3 Hz, 2H), 6.91 (t, J = 6.2 Hz, 2H), 6.76 (t, J = 9.0 Hz, 2H). ^{13}C NMR (101 MHz, DMSO-d_6) δ 169.50, 169.39, 167.13, 167.01, 166.37, 160.32 (dd, J = 238.4 Hz, J = 12.1 Hz), 150.32, 148.87, 144.36, 139.24, 133.34, 130.64 (d, J = 10.8 Hz), 129.69, 127.85, 127.12, 124.66, 123.85, 123.51, 121.16, 108.88 (d, J = 22.7 Hz), 105.52 (dd, J = 33.3 Hz, J = 25.3 Hz). Anal. Calcd. for $C_{41}H_{24}F_4IrN_6$: C, 48.57; H, 2.39; N, 8.29. Found: C, 48.63; H, 2.37; N, 8.25. MS (ESI) m/z: calcd for $[C_{41}H_{24}F_4IrN_6]^+$, 869.1628; found, 869.1655 $[M\text{-}PF_6]^+$.

$[(F_{3,5}piq)_2Ir(pip)](PF_6)$ (**6**): 0.31 g (0.27 mmol) of $[(F_{3,5}piq)_2Ir(\mu\text{-}Cl)]_2$ and 0.18 g (0.62 mmol) of pip, and 0.53 g (2.88 mmol) of KPF_6 gave 0.41 g orange powder. Yield: 73%. ^{1}H NMR (400 MHz, DMSO-d_6) δ 9.11 (d, J = 8.1 Hz, 2H), 8.28 (d, J = 8.1 Hz, 2H), 8.16 (d, J = 4.9 Hz, 2H), 8.12–8.06 (m, 3H), 8.05–7.97 (m, 4H), 7.91 (t, J = 7.8 Hz, 3H), 7.78 (d, J = 4.3 Hz, 1H), 7.49 (d, J = 5.6 Hz, 2H), 7.35–7.25 (m, 2H), 7.02 (t, J = 6.6 Hz, 2H), 6.96–6.90 (m, 2H), 5.90–5.84 (m, 2H). ^{13}C NMR (101 MHz, DMSO-d_6) δ 166.95, 166.83, 162.82, 159.78 (dd, J = 238.4 Hz, J = 12.1 Hz),153.48, 149.53, 149.45, 149.37, 149.27, 149.17, 144.36, 141.81, 136.90, 133.50, 132.56, 131.02, 130.16, 129.82 (d, J = 8.1 Hz), 128.09, 127.15, 126.56, 126.17, 126.03, 122.80, 114.05 (d, J = 23.2 Hz), 106.12 (d, J = 24.2 Hz). Anal. Calcd. for $C_{49}H_{28}F_4IrN_6$: C, 52.83; H, 2.53; N, 7.54. Found: C, 53.04; H, 2.64; N, 7.41. MS (ESI) m/z: calcd for $[C_{49}H_{28}F_4IrN_6]^+$, 969.1941; found, 969.1990 $[M\text{-}PF_6]^+$.

$[(F_{3,5}ppy)_2Ir(tfpip)](PF_6)$ (**7**): 0.31 g (0.27 mmol) of $[(F_{3,5}ppy)_2Ir(\mu\text{-}Cl)]_2$ and 0.18 g (0.62 mmol) of tfpip, and 0.53 g (2.88 mmol) of KPF_6 gave 0.41 g yellow powder. Yield: 67%. ^{1}H NMR (400 MHz, DMSO-d_6) δ 9.22 (d, J = 8.1 Hz, 2H), 8.53 (d, J = 7.8 Hz, 2H), 8.29 (dd, J = 8.0, J = 4.0 Hz, 4H), 8.14–8.07 (m, 2H), 8.04 (d, J = 8.1 Hz, 2H), 7.92 (d, J = 9.7 Hz, 2H), 7.85 (t, J = 7.7 Hz, 2H), 7.43 (d, J = 5.4 Hz, 2H), 6.91 (t, J = 6.6 Hz, 2H), 6.76 (t, J = 9.4 Hz, 2H). ^{13}C NMR (101 MHz, DMSO-d_6) δ 169.38, 167.12, 166.37, 166.33, 159.20, 159.08, 152.28, 150.31, 148.95, 148.67, 144.56, 139.85, 139.25, 133.37, 127.78 (d, J = 31.3 Hz), 126.67, 124.66, 121.17, 108.88 (d, J = 20.2 Hz), 105.53 (dd, J = 33.2 Hz, J = 24.4 Hz). Anal. Calcd. for $C_{42}H_{23}F_7IrN_6$: C, 46.63; H, 2.14; N, 7.77. Found: C, 46.74; H, 2.13; N, 7.50. MS (ESI) m/z: calcd for $[C_{42}H_{23}F_7IrN_6]^+$, 937.1502; found, 937.1535 $[M\text{-}PF_6]^+$.

$[(F_{3,5}piq)_2Ir(tfpip)](PF_6)$ (**8**): 0.31 g (0.27 mmol) of $[(F_{3,5}piq)_2Ir(\mu\text{-}Cl)]_2$ and 0.18 g (0.62 mmol) of tfpip, and 0.53 g (2.88 mmol) of KPF_6 gave 0.41 g orange powder. Yield: 67%. ^{1}H NMR (400 MHz, DMSO-d_6) δ 14.42 (s, 1H), 9.23 (d, J = 8.2 Hz, 2H), 9.03 (d, J = 8.3 Hz, 2H), 8.31 (d, J = 5.1 Hz, 4H), 8.21 (d, J = 10.5 Hz, 2H), 8.10 (s, 2H), 8.00 (d, J = 7.6 Hz, 2H), 7.90 (t, J = 8.3 Hz, 4H), 7.67 (d, J = 6.7 Hz, 2H), 7.62 (d, J = 6.5 Hz, 1H), 7.39 (s, 3H), 6.86 (d, J = 9.1 Hz, 2H). ^{13}C NMR (101 MHz, DMSO-d_6) δ 169.32, 166.96, 166.84, 158.53, 149.53, 149.45, 149.37, 149.28, 149.08, 144.45, 141.80, 136.90, 133.48, 132.56, 130.16, 128.09, 127.63, 126.64 (d, J = 14.1 Hz), 126.24,

126.03, 122.80, 114.05 (d, J = 22.2 Hz), 105.96 (dd, J = 32.3 Hz, J = 24.2 Hz).. Anal. Calcd. for $C_{50}H_{27}F_7IrN_6$: C, 50.81; H, 2.30; N, 7.11. Found: C, 51.09; H, 2.58; N, 6.87. MS (ESI) m/z: calcd for $[C_{50}H_{27}F_7IrN_6]^+$, 1037.1815; found, 1037.1879 $[M\text{-}PF_6]^+$.

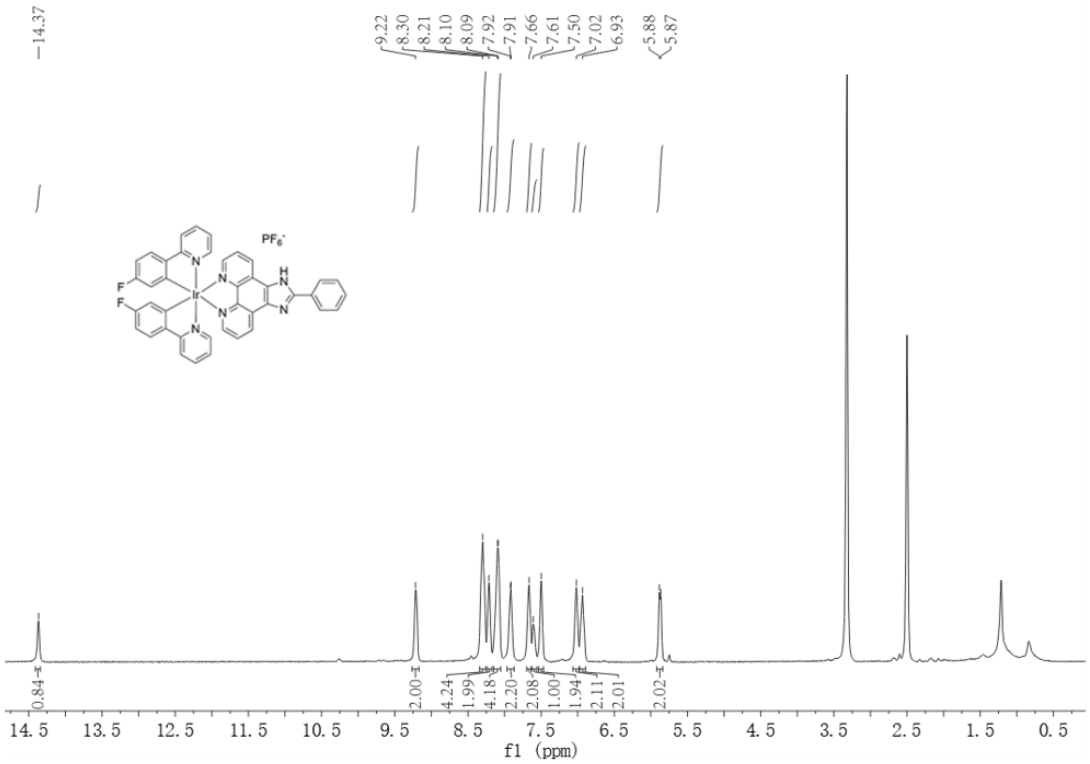

Fig. S1. The ^{1}H NMR spectrum of the complex **1**.

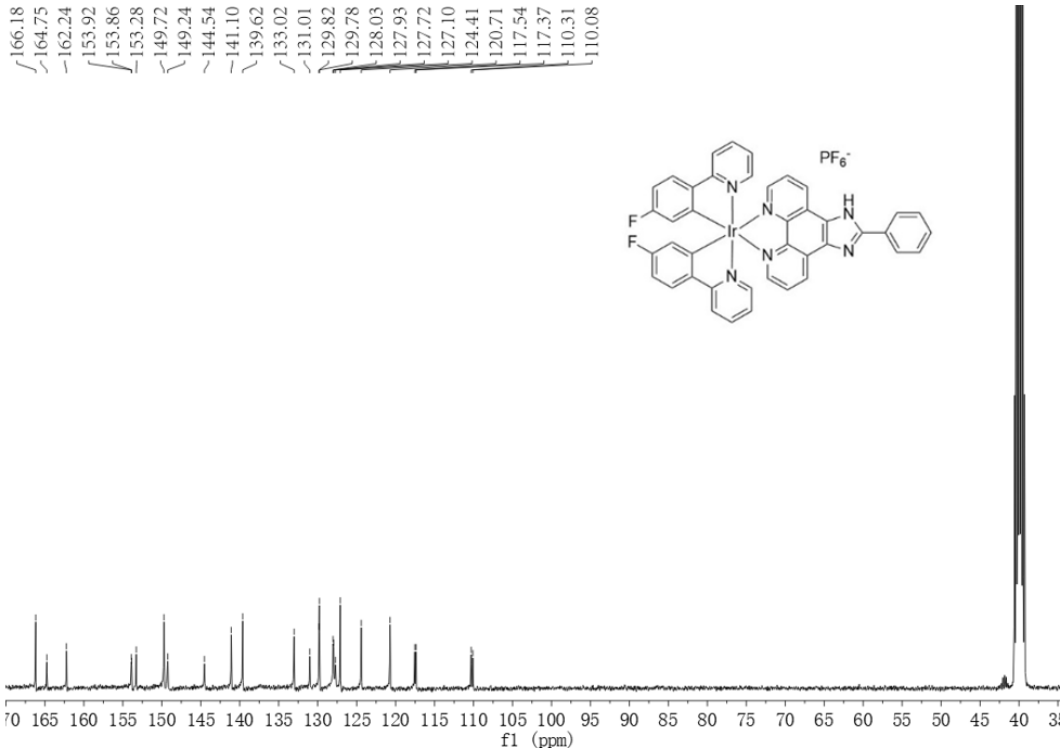

Fig. S2. The ^{13}C NMR spectrum of the complex **1**.

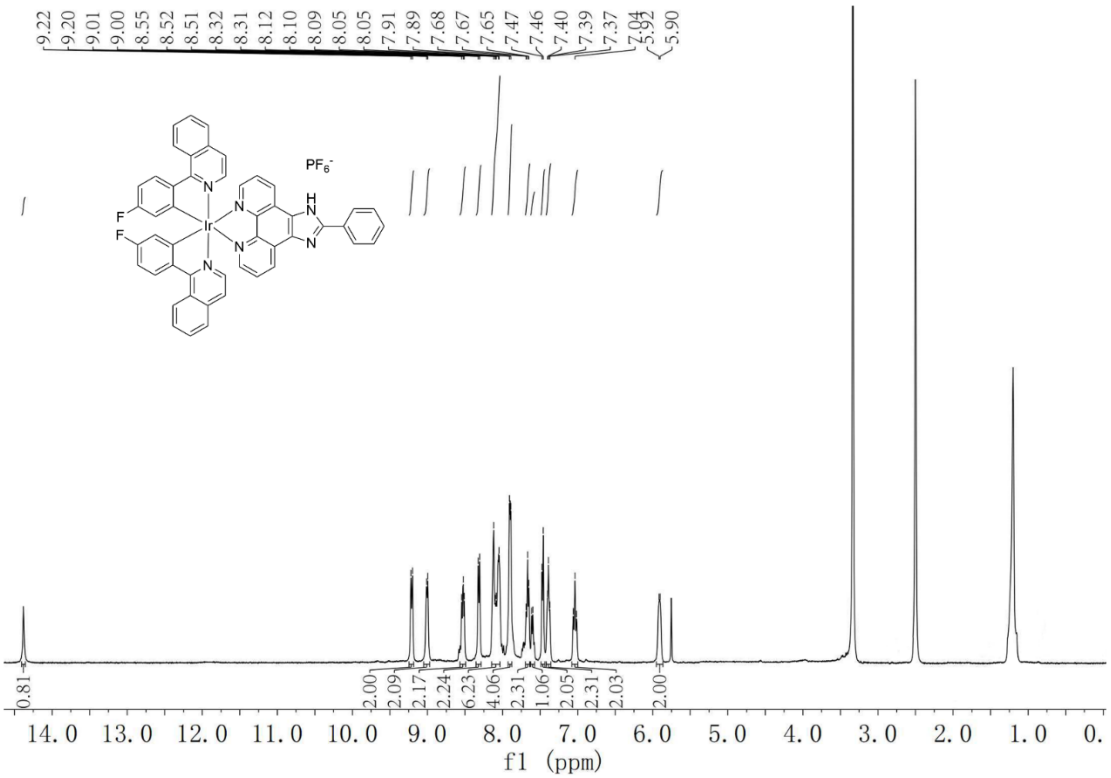

Fig. S3. The ^{1}H NMR spectrum of the complex **2**.

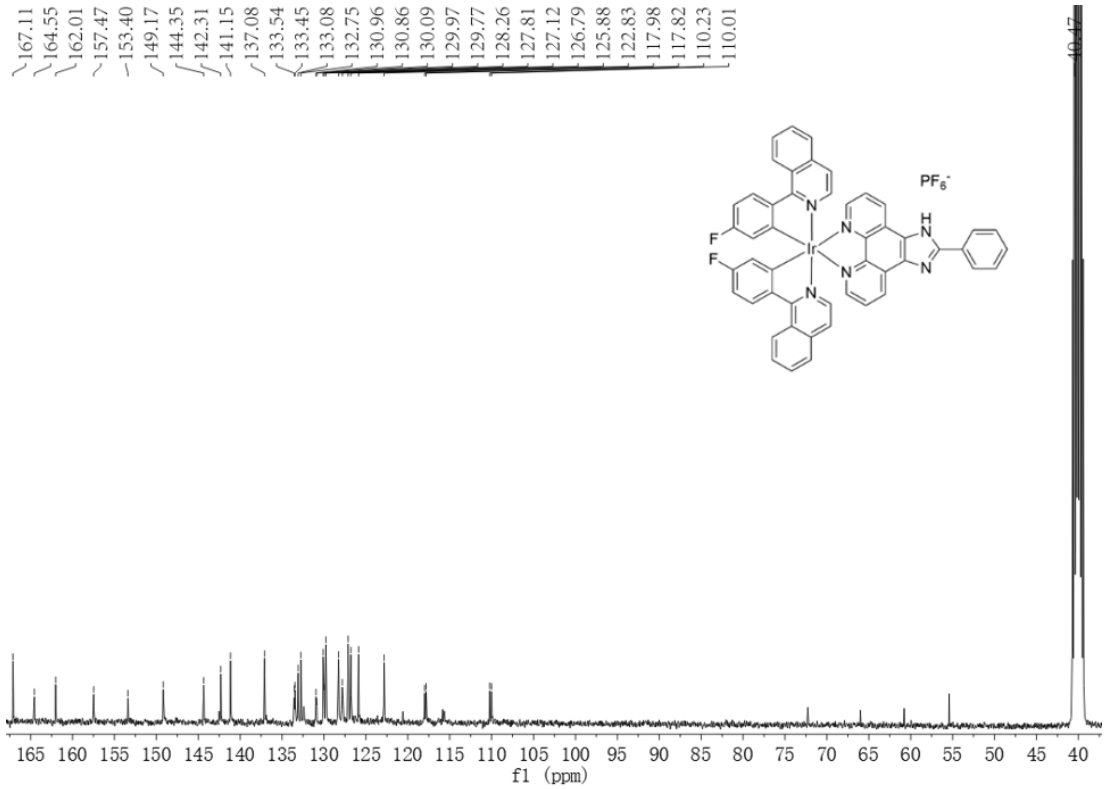

Fig. S4. The ^{13}C NMR spectrum of the complex **2**.

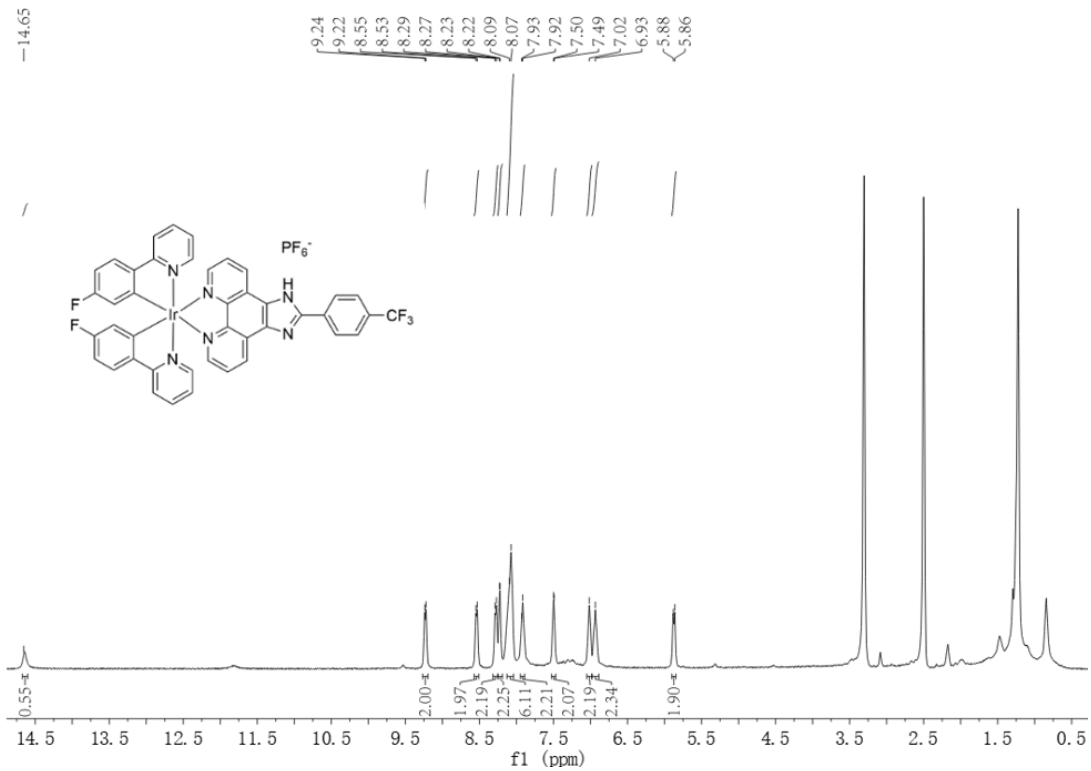

Fig. S5. The ^{1}H NMR spectrum of the complex **3**.

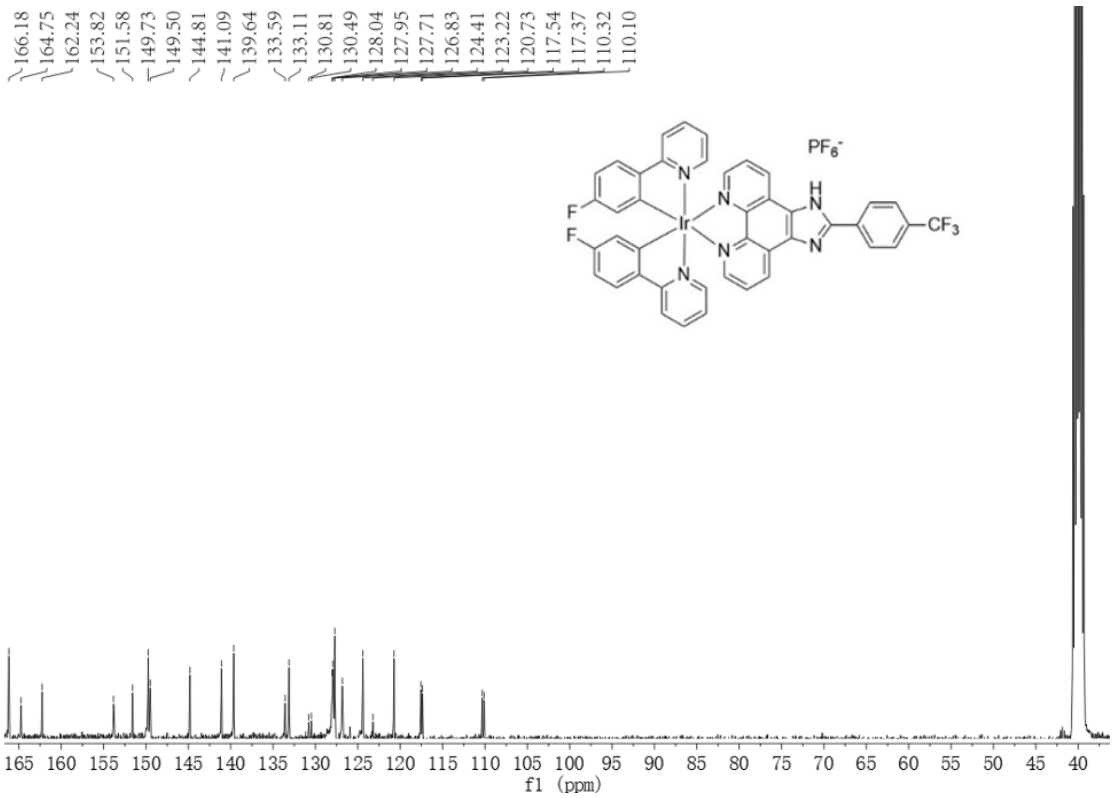

Fig. S6. The ^{13}C NMR spectrum of the complex **3**.

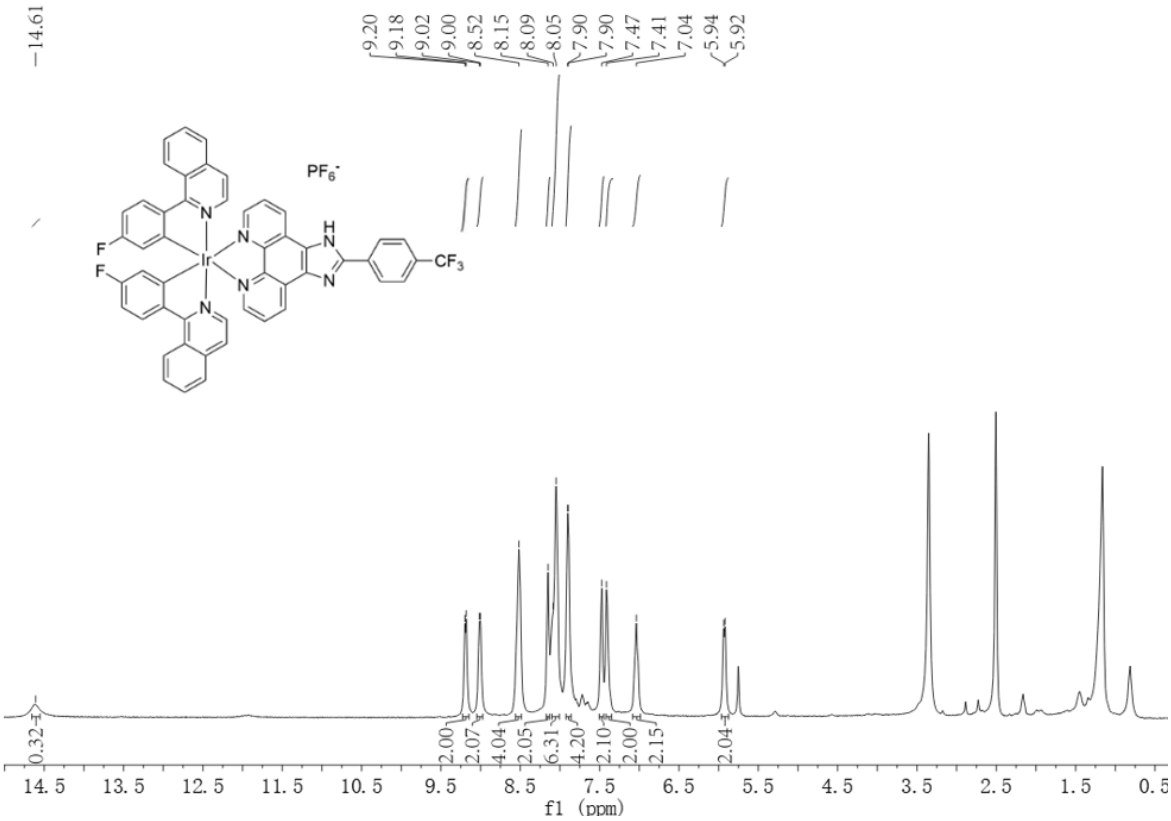

Fig. S7. The ^{1}H NMR spectrum of the complex **4**.

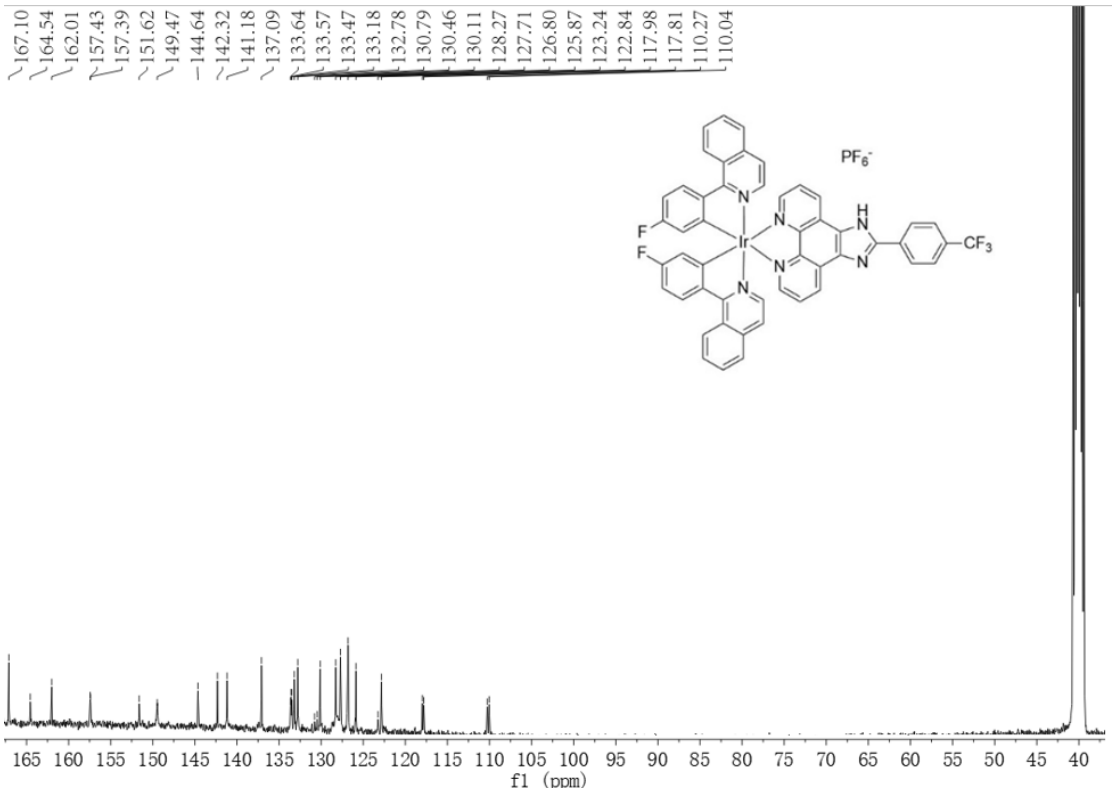

Fig. S8. The ^{13}C NMR spectrum of the complex **4**.

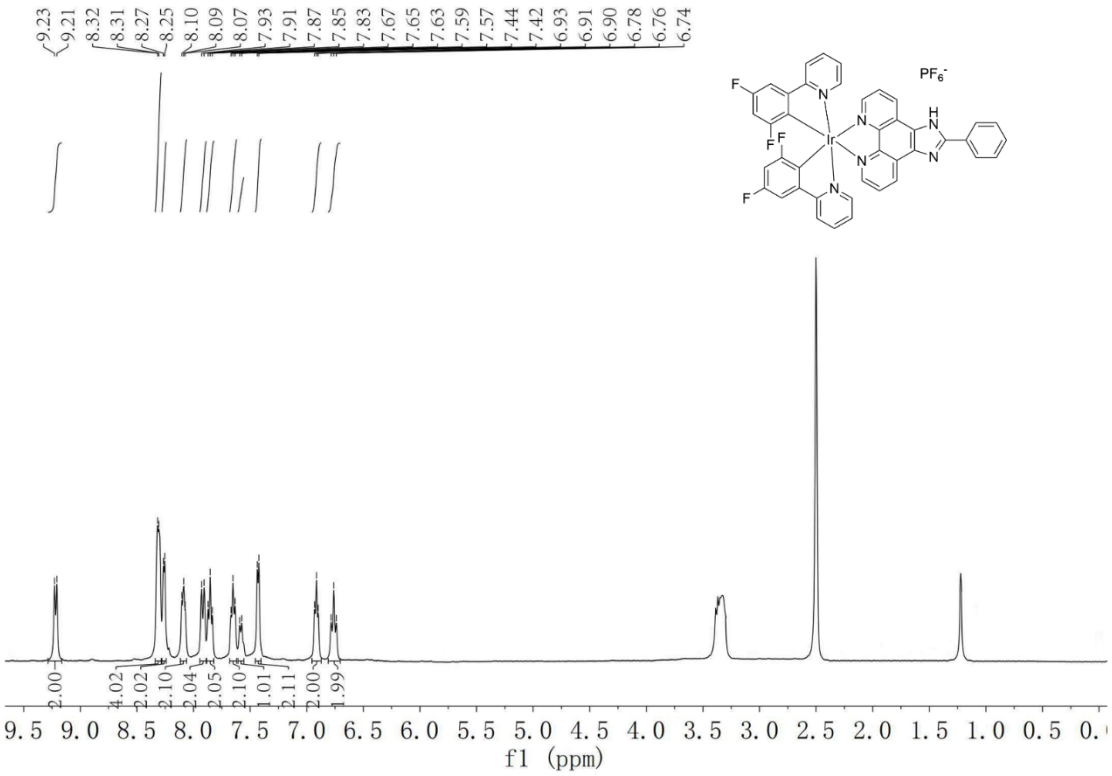

Fig. S9. The ^{1}H NMR spectrum of the complex **5**.

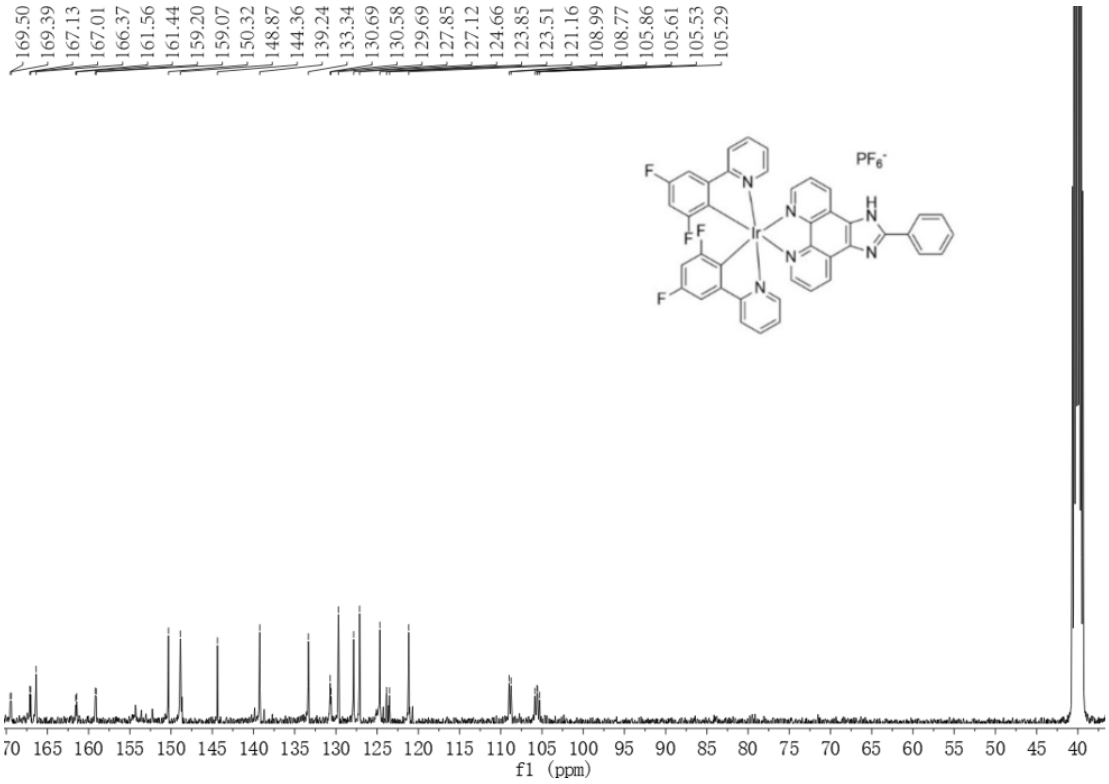

Fig. S10. The ^{13}C NMR spectrum of the complex **5**.

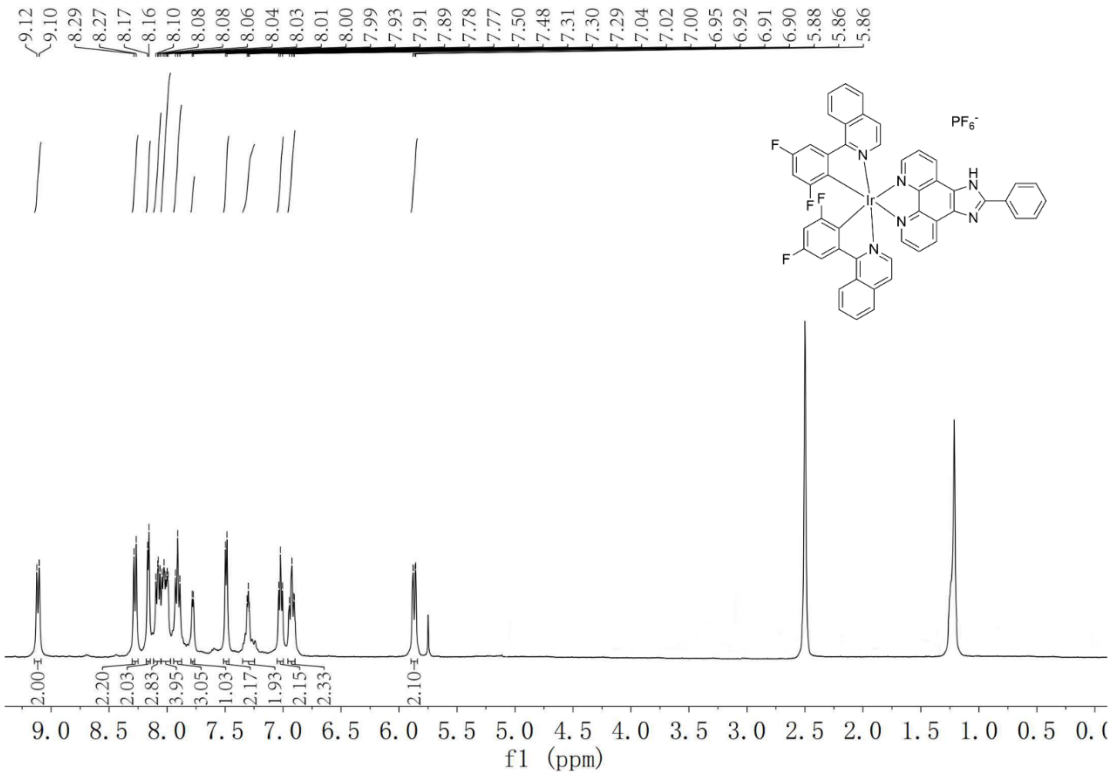

Fig. S11. The ^{1}H NMR spectrum of the complex **6**.

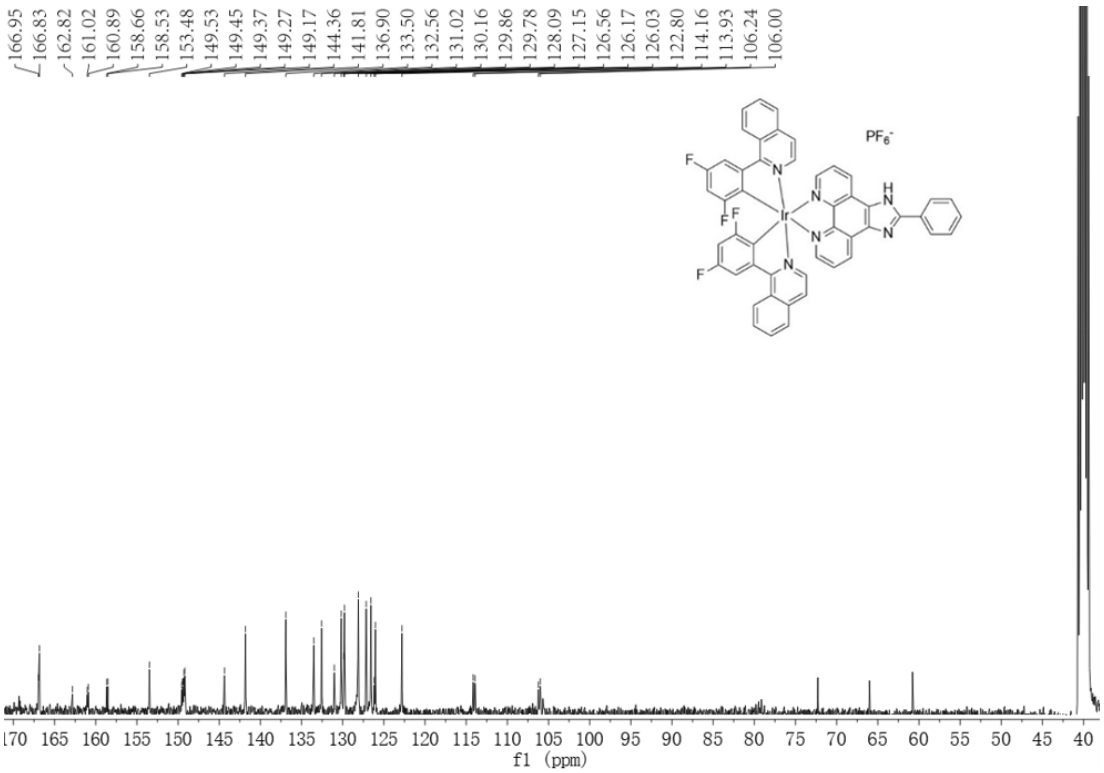

Fig. S12. The ^{13}C NMR spectrum of the complex **6**.

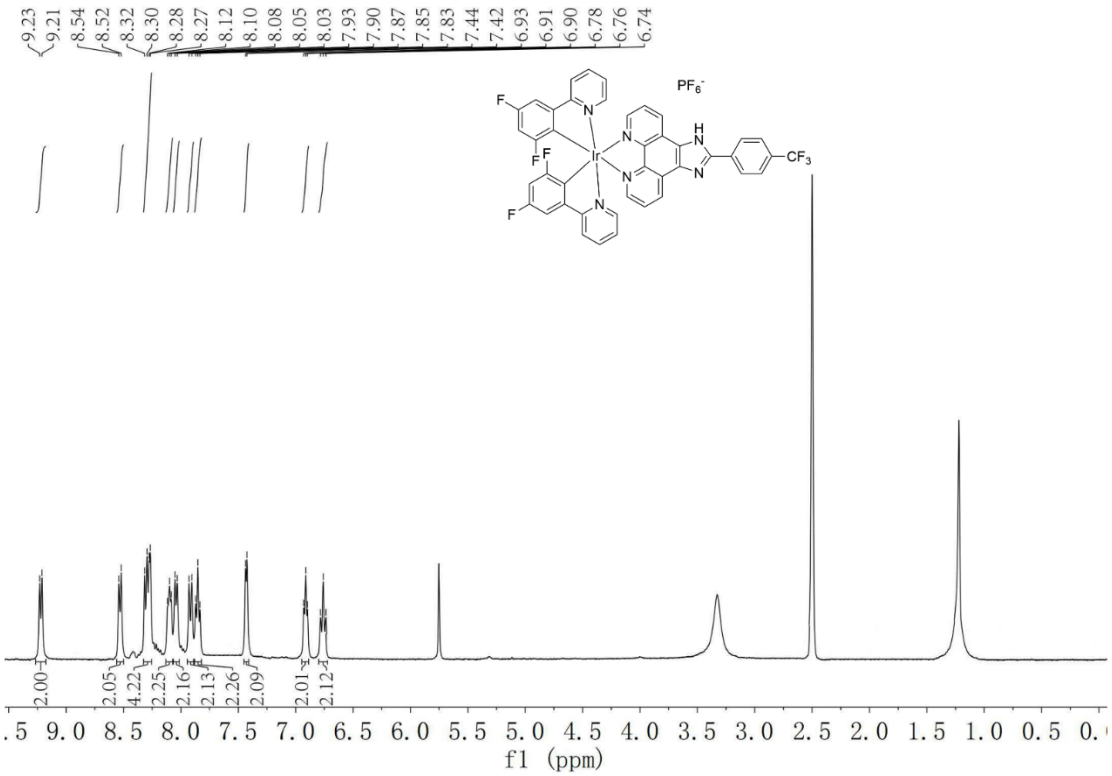

Fig. S13. The ^{1}H NMR spectrum of the complex **7**.

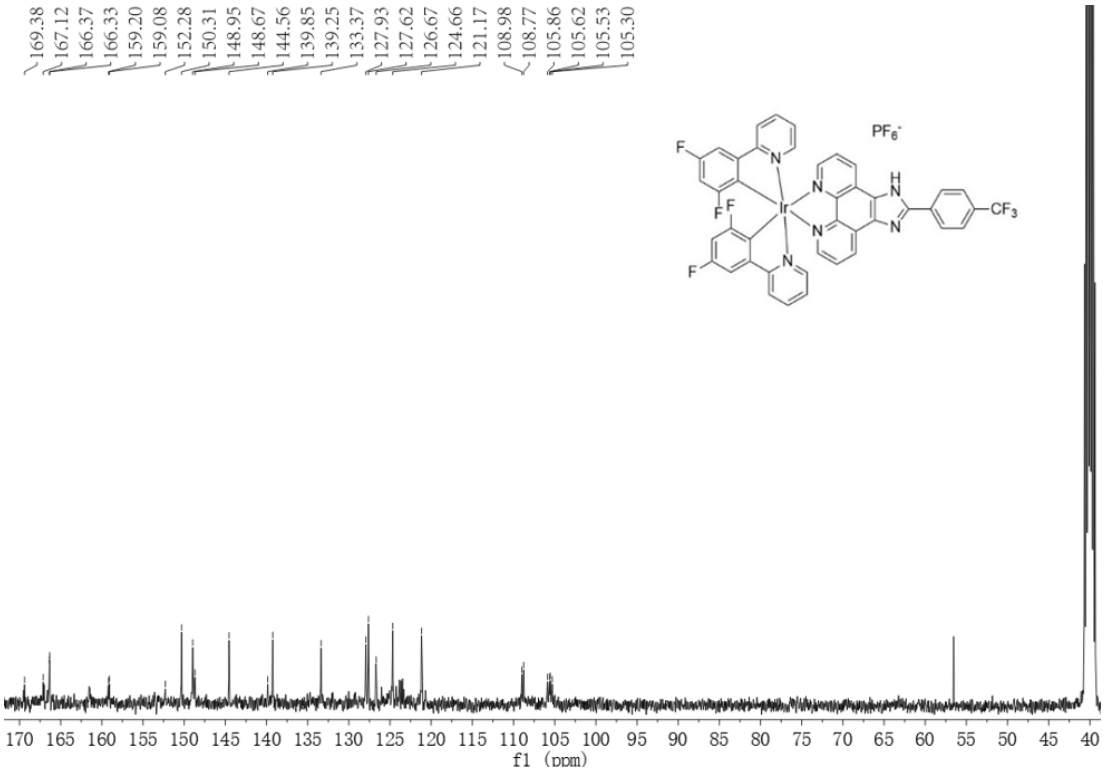

Fig. S14. The ^{13}C NMR spectrum of the complex **7**.

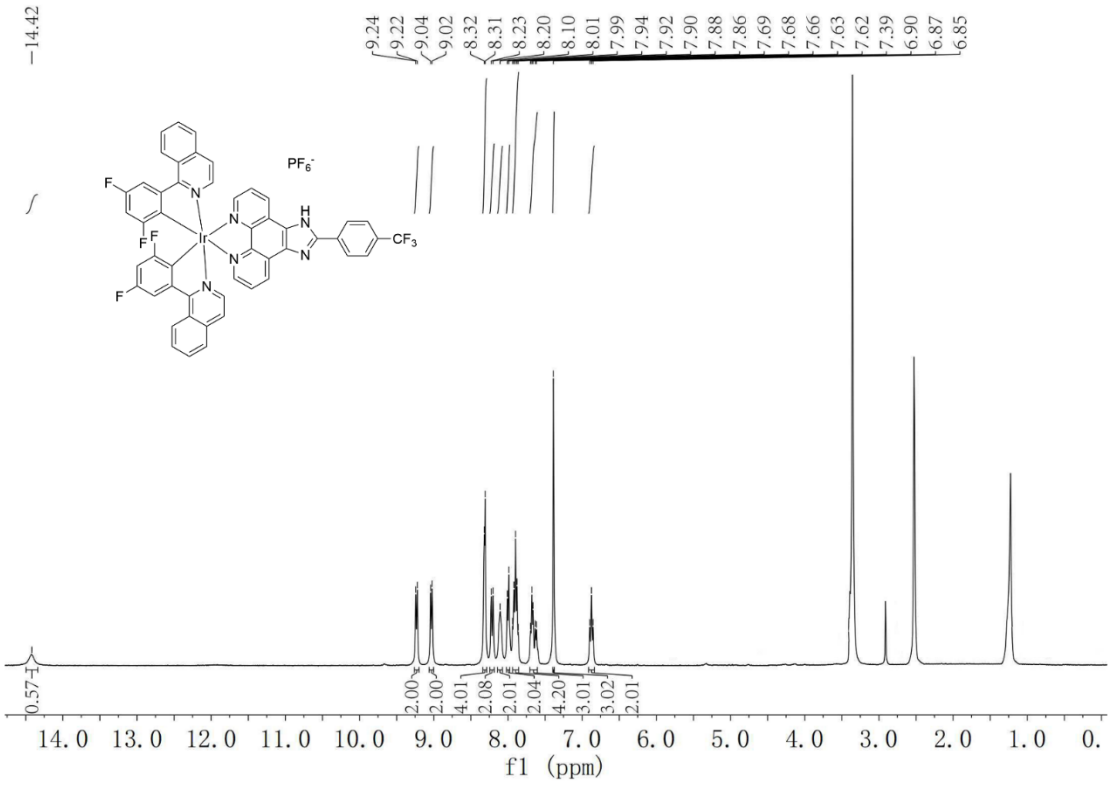

Fig. S15. The ^{1}H NMR spectrum of the complex **8**.

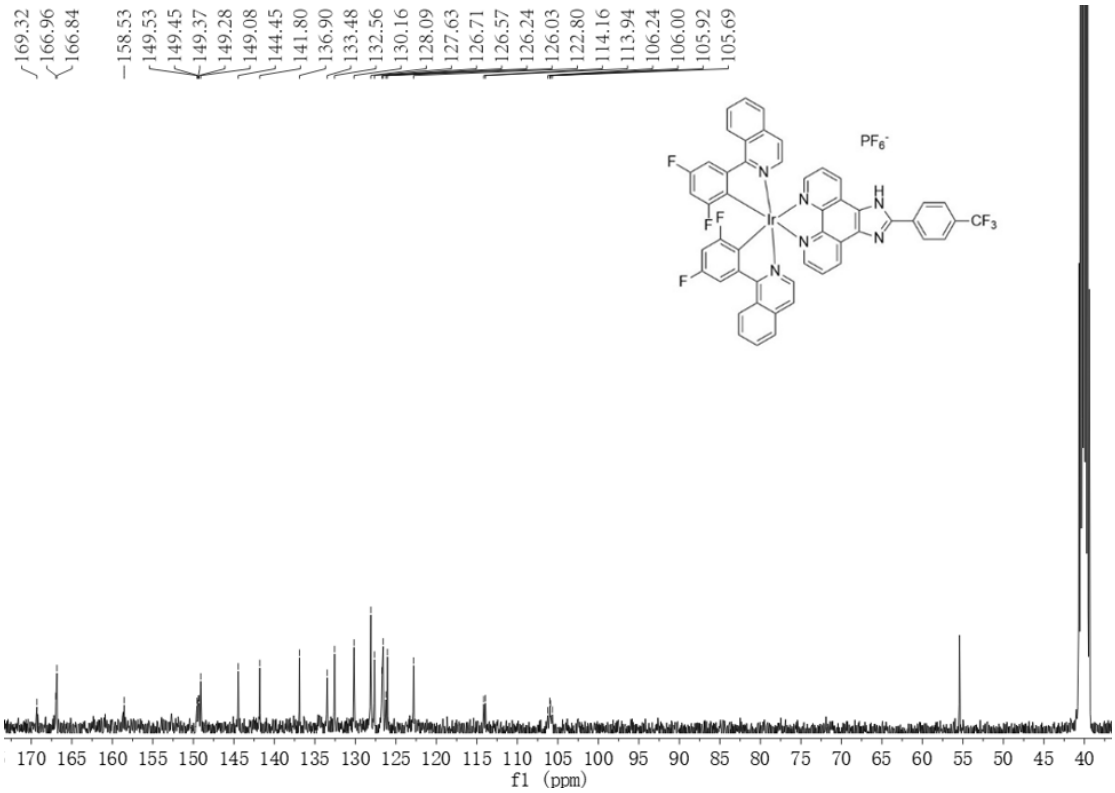

Fig. S16. The ^{13}C NMR spectrum of the complex **8**.

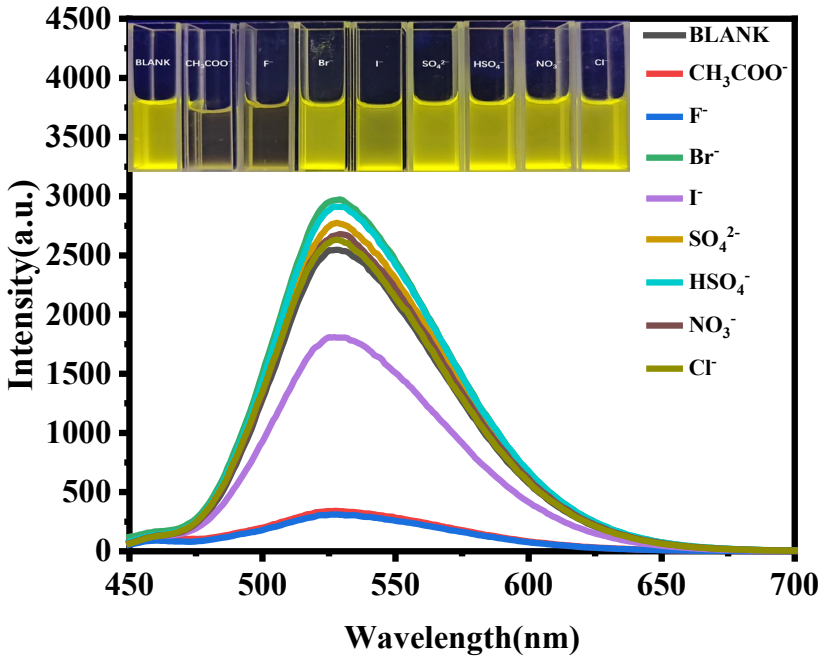

Fig. S17. Photoluminescence spectra of **1** upon addition of various anions (3.0 equiv.) in acetonitrile solution.

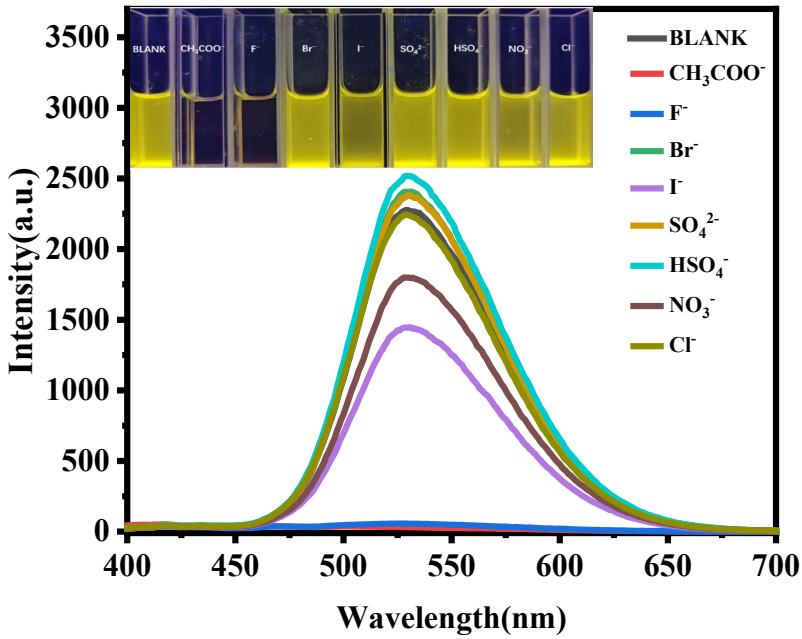

Fig. S18. Photoluminescence spectra of **5** upon addition of various anions (3.0 equiv.) in acetonitrile solution.

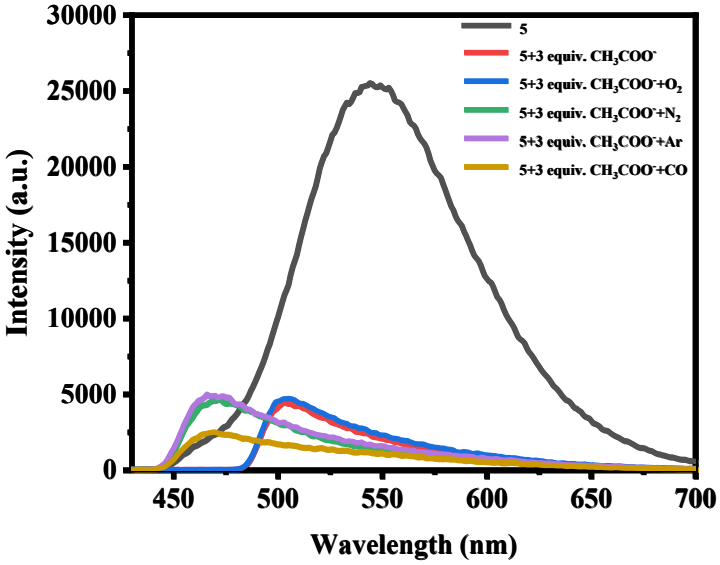

Fig. S19. The phosphorescence responses of complexes **5** in the presence of CH_3COO^- and then bubbling excess O_2, N_2, Ar, and CO gas.

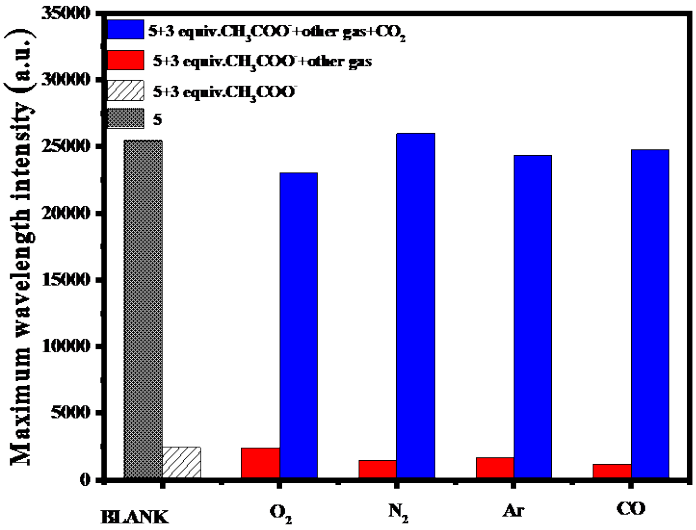

Fig. S20. The anti-interference experiment results of complex **5** in the presence of CH_3COO^- for sensing CO_2.

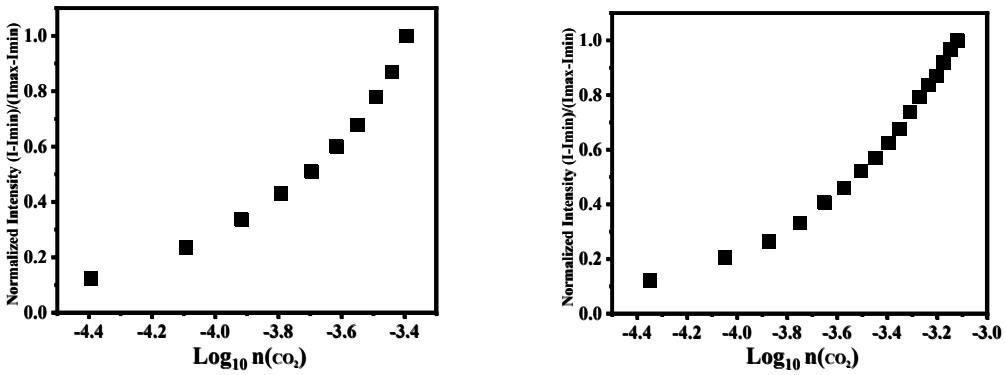

Fig. S21. Phosphorescence intensity change of **1−CH_3COO^-** (left) and complex **5−CH_3COO^-** symstem (5 μM) upon bubbling with various quantities of CO_2.

I_{min} represent the Phosphorescence intensity (at 534/536 nm) of **1/5−CH_3COO^-**

I_{max} represent the fluorescence intensity (at 534/536 nm) of **1/5−CH_3COO^-** upon bubbling with 10/17 mL CO_2.

The detection limit was calculated to be about 2.30×10^{-5} M and 2.28×10^{-5} M.[1, 2]

Table S1. The frontier orbital energy and electron density distribution of complexes **1**–**8**.

Complex	orbital	Energy (eV)	E_g (eV)	Composition%		
				cyclometalated ligand	Ir	ancillary ligand
1	HOMO−1	−6.109		1.93	4.91	93.16
	HOMO	−5.791	3.63	53.15	43.57	3.29
	LUMO	−2.428		2.38	3.84	93.78
	LUMO+1	−2.051		1.54	0.66	97.79
	LUMO+2	−1.765		92.02	4.99	3.00
2	HOMO−1	−6.055		74.91	11.90	13.18
	HOMO	−5.755	3.32	57.77	39.67	2.56
	LUMO	−2.434		9.21	3.36	87.44
	LUMO+1	−2.260		86.20	4.59	9.21
	LUMO+2	−1.799		5.27	1.21	93.53
3	HOMO−1	−6.237		21.48	11.54	66.99
			3.42			
	HOMO	−5.797		53.26	43.45	3.29
	LUMO	−2.458		2.29	3.72	93.99
	LUMO+1	−2.130		1.27	0.68	98.06
	LUMO+2	−1.799		5.27	1.21	93.53
4	HOMO−1	−6.065		86.79	10.50	2.71
	HOMO	−5.762	3.30	57.92	39.52	2.55
	LUMO	−2.462		7.56	3.33	89.11
	LUMO+1	−2.266		87.90	4.49	7.60
	LUMO+2	−2.139		67.43	4.55	28.02
5	HOMO−1	−6.139		0.96	3.18	95.86
	HOMO	−5.782	3.30	53.11	43.84	3.05
	LUMO	−2.483		2.41	3.69	93.90
	LUMO+1	−2.097		4.23	0.93	94.84
	LUMO+2	−1.889		91.88	4.68	3.44
6	HOMO−1	−6.137		0.98	3.47	95.55
	HOMO	−5.772	3.28	55.45	41.97	2.58

Table S1 (continuation)

	LUMO	−2.493		10.86	3.11	86.03
	LUMO+1	−2.355		83.83	4.44	11.73
	LUMO+2	−2.262		91.10	5.26	3.64
7	HOMO−1	−6.282		2.03	5.83	92.14
	HOMO	−5.789	3.28	53.18	43.76	3.06
	LUMO	−2.513		2.34	3.59	94.07
	LUMO+1	−2.169		2.56	0.81	96.62
	LUMO+2	−1.895		91.00	4.72	4.28
8	HOMO−1	−6.065		86.79	10.50	2.71
	HOMO	−5.762	3.26	57.92	39.52	2.55
	LUMO	−2.462		7.56	3.33	89.11
	LUMO+1	−2.266		87.90	4.49	7.60
	LUMO+2	−2.139		67.43	4.55	28.02

Table S2. Main experimental and calculated optical transitions of complexes **1**–**8**

Complex	Orbital Excitation	Transitions	Nature of transition	Oscillation strength	Calcd (nm)	Exptl (nm)
1	HOMO−1→LUMO	MLCT /LLCT	Ir(dπ)/L_{fppy}(π)→L_{fppy}(π*)	0.1310	400	396
2	HOMO→LUMO+1	MLCT /LLCT	Ir(dπ)/L_{fpiq}(π)→L_{fpiq}(π*)	0.1033	439	411
3	HOMO−1→LUMO	MLCT /LLCT	Ir(dπ)/L_{fppy}(π)→L_{fppy}(π*)	0.1817	389	398
4	HOMO→LUMO+1	MLCT /LLCT	Ir(dπ)/L_{fpiq}(π)→L_{fpiq}(π*)	0.1049	404	439
5	HOMO−1→LUMO	MLCT /LLCT	Ir(dπ)/L_{dfppy}(π)→L_{dfppy}(π*)	0.1167	403	399
6	HOMO→LUMO+1	MLCT /LLCT	Ir(dπ)/L_{dfpiq}(π)→L_{dfpiq}(π*)	0.0815	454	424
7	HOMO−1→LUMO	MLCT /LLCT	Ir(dπ)/L_{dfppy}(π)→L_{dfppy}(π*)	0.1621	391	398
8	HOMO→LUMO+1	MLCT /LLCT	Ir(dπ)/L_{dfpiq}(π)→L_{dfpiq}(π*)	0.0833	454	421

Table S3. The coordination geometry used to detect CO_2 and its corresponding detection limits

Complex	Detection limits	Response
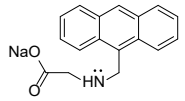	2 ppm	Turn on [3]
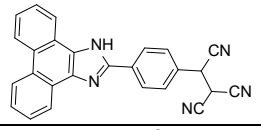	1.06×10^{-6} mol/L	Turn on [4]
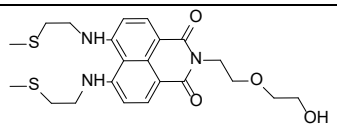	2.04×10^{-7} mol/L	Turn on [5]
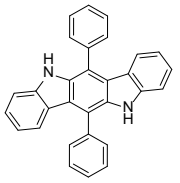	1.07×10^{-6} mol/L	Turn on [6]
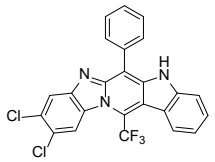	4.1×10^{-7} M	Turn on [7]
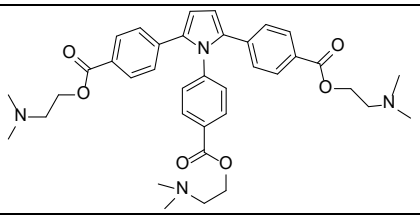	0.031%	Turn off [8]
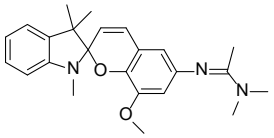	——	Color change [9]
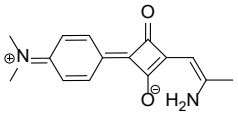	——	Turn on [10]

Table S3. (continuation)

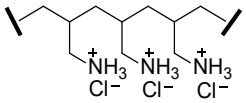	2 ppm	Turn off [11]
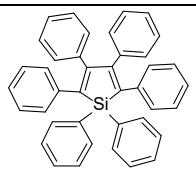	——	Turn on [12]
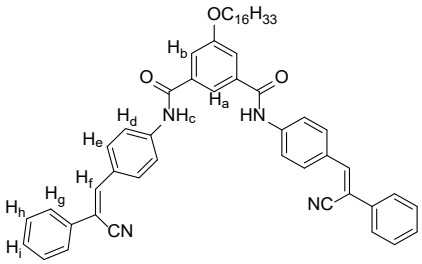	4.5 ppm	Turn off [13]
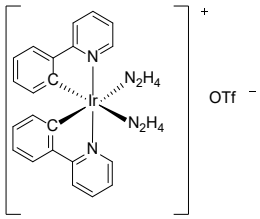	——	Sphere shift [14]
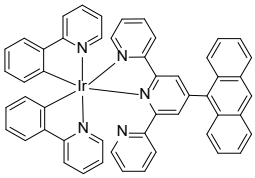	——	Turn on [15]
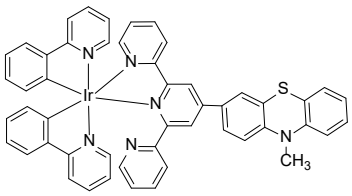	——	Turn on [15]
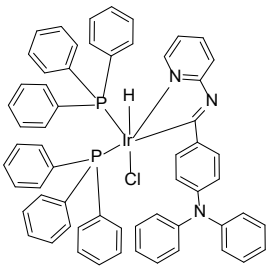	——	Turn on [16]

References

1 M. Shortreed, R. Kopelman, M. Kuhn and B. Hoyland, *Anal. Chem.*, 1996, **68**, 1414-1418.

2 Z. Guo, N. R. Song, J. H. Moon, M. Kim, E. J. Jun, J. Choi, J. Y. Lee, C. W. Bielawski, J. L. Sessler and J. Yoon, *J. Am. Chem. Soc.*, 2012, **134**, 17846-17849.

3 S. Kang, J. Kim, J. H. Park, C. K. Ahn, C. H. Rhee and M. S. Han, *Dyes Pigm.*, 2015, **123**, 125-131.

4. R. Ali, S. S. Razi, M. Shahid, P. Srivastava and A. Misra, *Spectrochim. Acta, Part A*, 2016, **168**, 21-28.

5. M. Lee, S. Jo, D. Lee, Z. C. Xu and J. Yoon, *Dyes Pigm.*, 2015, **120**, 288-292.

6. S. Y. Chen, H. Yu, C. Zhao, R. Hu, J. Zhu and L. Li, *Sens. Actuators, B*, 2017, **250**, 591-600.

7. M. Ishida, P. Kim, J. Choi, J. Yoon, D. Kim and J. L. Sessler, *Chem. Commun.*, 2013, **49**, 6950-6952.

8. H. Wang, D. D. Chen, Y. H. Zhang, P. Liu, J. B. Shi, X. Feng, B. Tong and Y. P. Dong, *J. Mater. Chem. C*, 2015, **3**, 7621-7626.

9. T. A. Darwish, R. A. Evans, M. James and T. L. Hanley, *Chem. Eur. J.*, 2011, **17**, 11399-11404.

10. J. Q. Sun, B. F. Ye, G. M. Xia, X. H. Zhao and H. M. Wang, *Sens. Actuators, B*, 2016, **233**, 76-82.

11. M. Hamer, J. M. Lázaro-Martínez and I. N. Rezzano, *Sens. Actuators, B*, 2016, **237**, 905-911.

12. Y. Liu, Y. H. Tang, N. N. Barashkov, I. S. Irgibaeva, J. W. Y. Lam, R. R. Hu, D. Birimzhanova, Y. Yu and B. Z. Tang, *J. Am. Chem. Soc.*, 2010, **132**, 13951-13953.

13. Y. Ma, M. Cametti, Z. Dzolic and S. M. Jiang, *J. Mater. Chem. C*, 2018, **6**, 9232-9237.

14. K. R. Schwartz and K. R. Mann, *Inorg. Chem.*, 2011, **50**, 12477-12485.

15. V. D. Singh, R. P. Paitandi, B. K. Dwivedi, R. S. Singh and D. S. Pandey, *Organometallics*, 2018, **37**, 3827-3838.

16. C. Climent, P. Alam, S. S. Pasha, G. Kaur, A. R. Choudhury, I. R. Laskar, P. Alemany and D. Casanova, *J. Mater. Chem. C*, 2017, **5**, 7784-7798.